Understanding Ductal Carcinoma In Situ Invasion using a Multiscale Agent-Based Model*

Joseph D. Butner, Vittorio Cristini, and Zhihui Wang, *Member, IEEE*

Abstract—**Ductal carcinoma in situ (DCIS) is commonly treated clinically through surgical resection. Although surgical options exist for resection, it is unclear which is optimal to reduce the likelihood of future invasive disease. This is further complicated by challenges in determining correct surgical margins from disease diagnostics, with mammographic imaging misidentifying surgical margins by as much as 2 cm vs. histological examination. We have implemented a three-dimensional, hybrid multiscale model of DCIS to study disease initiation and progression. In order to shed new light on current biological questions and clinical challenges surrounding the disease, we present here an improved version of this model, with more biologically relevant molecular signaling pathways, cell phenotype hierarchies, and duct architecture variation. In particular, a cell necrosis, lysis and calcification pathway has been incorporated into the model to help better understand the relationship between diagnostic imaging and the true extent of disease invasion. We observe that deficiencies in availability of molecular signaling molecules that upregulate cell proliferation may be overcome by dynamic shifts in phenotypic distributions within the disease mass. Hypoxia, necrosis, and calcification together functioned as a hypoxia relief mechanism, and were observed to maintain a consistent distance between the DCIS leading edge and the site of necrosis onset, providing insights for improving surgical margins.**

I. Introduction

DCIS is one of the most commonly diagnosed forms of breast cancer, composing around 20% of all diagnosis occurrences and affecting more than 63,000 women annually (in 2017) in the United States alone [1]. It is commonly treated surgically through lumpectomy (and occasionally full mastectomy), often with subsequent radiation or hormone therapy. Women with a history of DCIS are 8-10× more likely to develop invasive breast cancer [2], making improved detection and further understanding of disease initiation and progression of important clinical relevance.

It has been reported that DCIS is characterized by luminal epithelial cell loss-of-heterogeneity and invasion into the breast duct cavity, cell movement axially along the duct, and the presence of a necrotic/calcified core within larger ducts [3]. Breast cancers (including DCIS) are classified by estrogen receptor (ER), progesterone receptor (PR), and HER2 receptor status, which are all known to play key roles in disease progression. Among these, the presence of estrogen receptor α (referred to as ER positive: ER+) is found in as much as 75% of DCIS, exceeding incidences of PR+ and HER2+ disease. Progression from non-invasive DCIS into an invasive cancer phenotype is often associated with the presence or ER, and upwards of 70% of all breast tumors have been shown to be ER+ [4].

Epithelial cells in the mammary duct lumen gain the motility necessary to invade the duct cavity as DCIS through an epithelial to mesenchymal transition (EMT), which has been linked to a loss of ERα function [5]. Overstimulation in the estrogen/ER pathway upregulates proliferation within ER+ mammary epithelium in breast cancer populations and stimulates an epithelial to stromal downstream cascade to the estrogen receptor negative (ER−) subpopulation through upregulation of membrane-bound amphiregulin (AREG) production in ER+ cells [5]. AREG is cleaved via ADAM17 and released into the extracellular space, where it leaves to the surrounding stroma and binds to EGF, resulting in a stromal to epithelial cascade back into the mammary epithelium, in part through the fibroblast growth factor pathway (e.g., FGF2, FGF7), which upregulates proliferation within the ER− epithelial population [6].

We have been using a multiscale modeling approach to complement current experimental and clinical work in prevention, diagnosis, and treatment of cancer [7-13]. In particular, we have implemented a three-dimensional, lattice-free multiscale agent based model (ABM) of DCIS to study the early stages of DCIS duct invasion, which builds upon our previous work on the normal mammary gland pubertal development and post-menopausal DCIS initiation [14-16]. We have now made several significant improvements through the addition of cell density induced quiescence, hypoxia, necrosis, lysis, and calcification of lysed cytoplasmic contents. As our current focus is on the early stages of DCIS initiation, we model only a section of a single simulated mature mammary duct, approximated as a bilayered cylinder with outer myoepithelial (basal) and inner luminal layers, surrounding an open duct cavity. In our model, DCIS is initiated through a small population of cancer stem cells (CSCs) within the wall of the luminal (inner) layer, which may proliferate and generate stem and progenitor daughters. DCIS is prevalently composed of the luminal phenotype, and as such the outer myoepithelial layer does not contribute to the DCIS population in this model. Through signaling threshold limitations, cancer metabolism-induced oxygen limitations, and the stochastic nature of daughter phenotype selection and movement, we use the model to gain valuable insights into the cell population dynamics involved in early stage DCIS.

*This work has been supported in part by the National Science Foundation Grant DMS-1716737 (V.C., Z.W.), the National Institutes of Health (NIH) Grants 1U01CA196403 (V.C., Z.W.), 1U01CA213759 (V.C., Z.W.), 1R01CA226537 (V.C., Z.W.), 1R01CA222007 (V.C., Z.W.), and the Rochelle and Max Levit Chair in the Neurosciences (V.C.).

J.D.B., V. C. and Z.W. are with the Center for Precision Biomedicine, Brown Foundation Institute of Molecular Medicine, University of Texas Health Science Center at Houston McGovern Medical School, Houston, TX 77054, USA, and also with Department of Imaging Physics, University of Texas MD Anderson Cancer Center, Houston, TX 77230, USA (corresponding author, phone: 713-486-5425; fax: 713-796-9697; e-mail: Zhihui.Wang@uth.tmc.edu).

II. METHODS

A. Discrete Scale

Each cell in the mature duct and the DCIS population is represented as a discrete agent: a unique three-dimensional entity with its own spatial coordinates, phenotype, size, and phase in the cell cycle. Agents are implemented in a physics-based, lattice-free system, where they may move purely based on their interactions with their surroundings. Cell movement is determined by solution of the force balance the cell experiences from its surroundings, including displacement forces from neighboring cell movement or growth, cell-cell adhesion, viscous dampening from the surrounding fluid environment, and inelastic cell deformation (implemented as a coefficient of restitution, and not explicitly modeled). Cells are free to move within the constraints of this environment, but may not penetrate the mature duct (to model only stage zero DCIS) and may not occupy the same space as another agent.

Cell agents with a progenitor or stem phenotype simulate the cell cycle through a cycle of mitosis, growth, and preparation for the next mitosis event. Proliferative agents which have completed the last cell cycle (all cell cycles are 16 hours of time simulated based on values reported in the literature for mammary epithelium) may enter mitosis, provided that a series of checkpoints are satisfied, including sufficient local molecular concentrations to stimulate the mitosis event, adequate room to divide, and the agent is not hypoxic or necrotic. Upon mitosis, cytoplasmic volume is evenly divided between the daughters. Daughter phenotype is determined as shown in **Fig. 1**, with mitosis occurring either symmetrically or asymmetrically (daughters have same or different phenotype, respectively). Progenitor cells will undergo many proliferation cycles before becoming terminally differentiated [17], and those that exceed a proliferation cycle threshold will automatically divide into two differentiated daughters. CSCs in the population do not experience this proliferation threshold limit.

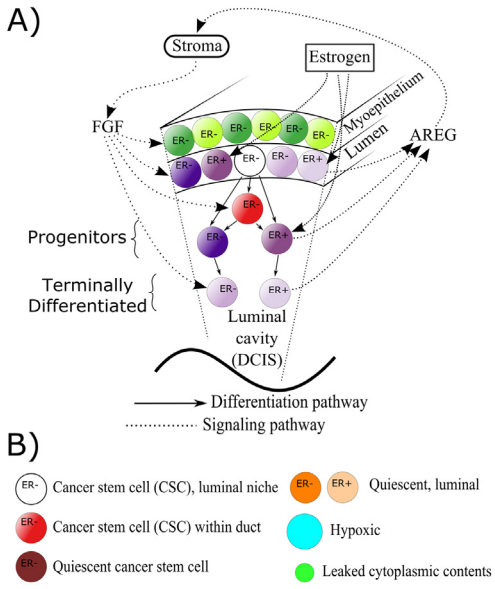

Fig. 1. Computational domain. A) Cross-section of a region of mature duct and cell hierarchy of DCIS invasion into luminal duct cavity. At simulation start, a CSC niche is seeded in the luminal layer (white); upon mitosis, one daughter is placed adjacently into the duct cavity according to hierarchy shown. Progenitors may give rise to progenitor or differentiated daughters as determined by proliferation threshold limits. B) Color scheme for quiescent, necrotic, and post-lysis leaked cytoplasmic contents.

Cancer cells experience increased oxygen consumption due to a glycolytic metabolism mechanism, which can result in localized hypoxic conditions. Agents which experience hypoxia longer than a threshold time (12 hours) become irreversibly necrotic, and subsequently undergo a cell death and lysis process. Agents swell to double their volume before plasma membrane rupture (6 hours), at which point their cytoplasmic contents are leaked into the duct cavity (for simplicity, modeled as a smaller agent 30% the volume of the pre-lysis agent volume); these will later become calcified.

B. Continuum Scale

Within the model, we solve molecular profiles for oxygen, estrogen, AREG, and FGF (**Fig. 1**), each of which is represented by a unique continuum solution. We note that these represent only a subset of literature-reported molecules that are known to play important roles in DCIS biology [5]. We assume these molecules may move freely through the computational domain, and are thus implemented via a Fick's law of diffusion. A unique solution for each molecule is obtained for each time step using finite element methods. Estrogen and oxygen are sourced from the capillary-delivered blood supply at the outer duct surface (not explicitly modeled, but assumed to be a large reservoir and thus roughly constant in concentration), and are imposed on the outer radial boundary as constant Dirichlet boundary conditions. AREG is produced internally in the duct by the ER+ population (both in the mature duct luminal layer and in the ER+ DCIS population), and may freely diffuse through the duct and out across the radial boundary into the stroma, which is accomplished numerically through far field homogenous Neumann boundary conditions on the outer duct radius. Stromal FGF production is upregulated by AREG stimulation; to this end we assume a 1:1 ratio between AREG entering the stroma and FGF reentering the duct at the following simulation time step, implemented numerically as a Dirichlet boundary condition where each node in the FGF solution is passed the value at that node from the AREG solution at the previous time step. To improve solution stability and accuracy, numerical solutions for each molecular profile are solved at a finer time resolution than the discrete agent based model.

C. Hybrid Modeling Method

At each time step in the simulation, agents interact with molecules in their microenvironment through feedback between the discrete and continuum portions of the model. Agents retrieve information about molecular concentrations at their location from the continuum solutions, and impose modifications on these solutions as they bind, metabolize, or produce the corresponding molecules. Mathematically, each agent approximates its local molecular concentration via barycentric interpolation from its nearest surrounding nodes in the continuum solution to its location (approximated as the agent center of mass), and agent induced changes to the

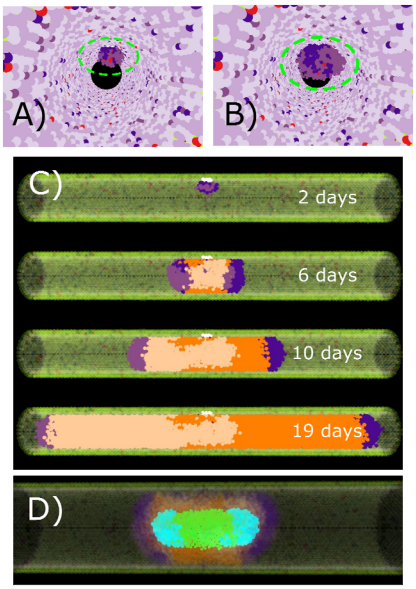

Fig. 2. Simulation output. A) DCIS invasion after 3.0 days (darker purple, circled) within a 100 µm radius, 1000 µm length duct section. B) DCIS mass shown in A grows larger as time progresses (5 days). C) Side view of DCIS growth in 50 µm radius, 1000 µm length duct shows duct invasion over increasing time (top to bottom). Quiescence due to cell density (orange) occurs at most highly populated region (center) of DCIS mass as cell population grows; while disease progression is spearheaded by non-quiescent leading edge (purple). D) Internal view of DCIS in larger (200 µm radius, 1000 µm length) duct shows necrotic (light blue) and lysed (bright green) regions along central duct axis.

local molecular concentrations are implemented into the continuum solutions as Dirac delta functions applied at the node nearest the agent's center of mass (a reasonable approximation achieved by ensuring mesh discretization size is on the same order as agent diameter). In this way, ER+ agents are stimulated via local estrogen concentration to produce AREG, which is added into the AREG continuum profile, and then may diffuse into the stroma and stimulate an analogous process of FGF production into the FGF continuum solution. This explicit mathematical feedback between scales results in a good representation of the oxygen availability and endocrine and paracrine signaling pathways, which we examine in closer detail in this work. The model was developed in C++, and includes functionality from several open-source packages, inducing Trilinos (Sandia National Lab), Boost, Bullet, FLANN, VTK, and OpenGL. All simulations and results presented were run (in 24–48 wall-clock hour serial runs) on the Lonestar 5 computer at Texas Advanced Computing Center (TACC), University of Texas at Austin [18].

III. Results and Discussion

We first investigated how the diameter of a mammary duct influences the early stages of DCIS progression by testing our model in several different sized ducts, of 25 µm, 50 µm, and 100 µm inner radii. Tests were performed in simulated ducts of 1,000 µm length and CSCs were seeded in a CSC niche within the luminal wall (composed of 5 adjacent CSCs in all cases). In order to isolate the effects of duct size from the influence of signaling pathways, agent sensitivity to molecular signaling was set to be minimal, ensuring molecular concentrations were sufficient to upregulate proliferation in all phenotypes and in all regions of the duct cavity.

At simulation start, the duct cavity is completely void of DCIS, with DCIS invasion initiated when one or more CSCs in the niche reaches the end of its current cell cycle and undergoes mitosis, placing a new DCIS progenitor or stem type daughter adjacent to itself but into the duct cavity and initiating DCIS invasion. At this early stage of invasion (see **Fig. 2A,B**), cell density is low surrounding the CSC niche and newly formed DCIS mass, allowing the DCIS population to undergo exponential growth (doubling in number each cell cycle; **Fig. 3**) until the cell mass becomes large enough that cells in center of the highly dense DCIS body experience a transition to cell density induced quiescence. We label this quiescent population orange, which is easily seen in **Fig. 2C**. Subsequent to the initiation of cell density induced quiescence, DCIS is advanced axially in both directions down the duct by a leading edge of highly proliferative cells, away from the location of disease initiation (leading edge shown in purple; **Fig. 2C**). This results in the leading edge being composed of a relatively consistent number of cells (found to be around 5-10 cell layers thick, depending on the stochastic events involved in cell proliferation and movement in the model), with linear ductal invasion rates and DCIS cell population number expansion rates spearheaded by this relatively consistent leading edge cell population (**Fig. 3**).

Hypoxia induced necrosis and lysis were only seen along the central duct axis in the 100 µm radius duct, the largest tested (**Fig. 2D**). Diffusion across shorter radial distances was able to overcome the increased oxygen consumption rates of cancer cell metabolism in the smaller 25 and 50 µm

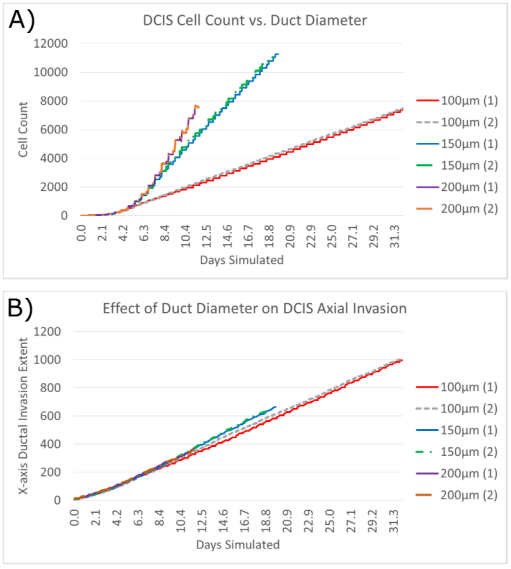

Fig. 3. Total DCIS cell count and axial invasion over time. Test were performed in duplicate to examine the effect of duct radius on A) DCIS cell count and B) DCIS axial invasion. In all tests performed, DCIS was initiated at time t=0 in a niche of 5 adjacent CSCs in the mature duct lumen. Tests showed consistent proliferation and invasion rates in both tests and in all duct radii. Cell populations increase exponentially at early times until the onset of cell density induced quiescence, resulting in a transition into liner population increases and axial invasion rates.

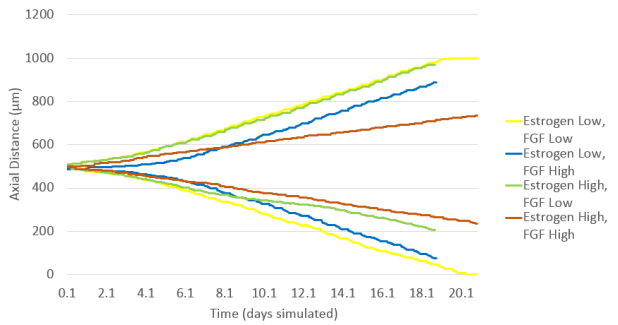

Fig. 4. Effect of molecular signaling sensitivity on DCIS axial invasion extent. Plots show the position of the cell farthest axially along the duct (CSC niche initiated at axial location 500 µm at time t=0). Thresholds were tested at low and high levels, with low threshold allowing cells to be stimulated into mitosis at low local molecular signaling concentrations. High thresholds resulted in reduced proliferation, lower total cell counts, and reduced axial invasion rates relative to low threshold behavior.

radius ducts, and extended periods of hypoxia and resultant necrosis did not occur in these cases. Necrotic cell death was seen to act as a hypoxia relief mechanism, reducing local oxygen metabolism in these locations. Viable DCIS population surrounding this region was 5-8 cells in thickness, consistent with biological observations [3].

We also sought to understand the effects of molecular signaling on DCIS invasion. This was accomplished by independent variation of cell sensitivity thresholding to estrogen and FGF, with low thresholds (i.e. cells have high sensitivity to signaling effects) allowing upregulation of mitosis at low molecular concentrations. Cell proliferation and disease progression were greatly impeded with simultaneous decrease in cell sensitivity to both estrogen and FGF (relative to the low threshold case), while results of independent variation of sensitivity to only one molecule at a time showed disease progression rates intermediary between the low and high sensitivity cases. Effects of elevated estrogen thresholds were more pronounced, likely because of its role upstream to AREG and FGF, and thus this restriction cascades downstream as well. Notably, when only one phenotype was proliferation limited by molecular signaling unavailability, a mixed phenotype population was able to overcome this limitation through emerging dominance of the non-limited phenotype, demonstrating one possible mechanism of DCIS adaptation to overcome limiting circumstances (this behavior was observed in the test shown in **Fig. 4** green curves: Estrogen High, FGF Low).

In our upcoming work, we will further calibrate the model against literature supported and experimentally measured parameters to more accurately represent the biology of the in vivo system, and use this platform to further analyze the underlying cell and molecular scale mechanisms involved in DCIS. Of particular interest, we will study how phenotypic diversity within the DCIS population allows the disease to adapt to limiting factors it may encounter (i.e., molecular deficits, high cell density, oxygen restrictions, etc.), shedding new lights on potential mechanisms to slow disease progression. Additionally, we will examine the relationship between DCIS progression and the development of axial calcification, allowing for accurate quantification of the link between imaging diagnostics (i.e. mammography) and the true disease extent, and helping to better define effective surgical resection boundaries.

ACKNOWLEDGMENT

We thank M Lewis and J Rosen (Baylor College of Medicine), J Lowengrub (UC Irvine), and Y-L Chuang (California State U, Northridge). We acknowledge support from the Methodist Hospital Research Institute (V.C.).

REFERENCES

[1] A. C. Society, "Breast Cancer Facts & Figures 2017-2018," American Cancer Society, Inc., 2017.

[2] M. A. Lopez-Garcia, F. C. Geyer, M. Lacroix-Triki *et al.*, "Breast cancer precursors revisited: molecular features and progression pathways," *Histopathology,* vol. 57, no. 2, pp. 171-92, Aug, 2010.

[3] N. A. Mayr, J. J. Staples, R. A. Robinson *et al.*, "Morphometric studies in intraductal breast carcinoma using computerized image analysis," *Cancer,* vol. 67, no. 11, pp. 2805-12, Jun 01, 1991.

[4] M. Moerkens, Y. Zhang, L. Wester *et al.*, "Epidermal growth factor receptor signalling in human breast cancer cells operates parallel to estrogen receptor α signalling and results in tamoxifen insensitive proliferation," *BMC Cancer,* vol. 14, pp. 283-283, 04/23, 2014.

[5] N. Gjorevski, and C. M. Nelson, "Integrated morphodynamic signalling of the mammary gland," *Nat Rev Mol Cell Biol,* vol. 12, no. 9, pp. 581-93, Aug 10, 2011.

[6] M. D. Sternlicht, and S. W. Sunnarborg, "The ADAM17-amphiregulin-EGFR axis in mammary development and cancer," *J Mammary Gland Biol Neoplasia,* vol. 13, no. 2, pp. 181-94, Jun, 2008.

[7] V. Cristini, E. Koay, and Z. Wang, *An Introduction to Physical Oncology: How Mechanistic Mathematical Modeling Can Improve Cancer Therapy Outcomes*: CRC Press, 2017.

[8] T. S. Deisboeck, Z. Wang, P. Macklin *et al.*, "Multiscale cancer modeling," *Annu Rev Biomed Eng,* vol. 13, pp. 127-55, Aug 15, 2011.

[9] Z. Wang, J. D. Butner, R. Kerketta *et al.*, "Simulating cancer growth with multiscale agent-based modeling," *Semin Cancer Biol,* vol. 30, pp. 70-8, Feb, 2015.

[10] Z. Wang, R. Kerketta, Y. L. Chuang *et al.*, "Theory and Experimental Validation of a Spatio-temporal Model of Chemotherapy Transport to Enhance Tumor Cell Kill," *PLoS Comput Biol,* vol. 12, no. 6, pp. e1004969, Jun, 2016.

[11] J. Pascal, E. L. Bearer, Z. Wang *et al.*, "Mechanistic patient-specific predictive correlation of tumor drug response with microenvironment and perfusion measurements," *Proc Natl Acad Sci U S A,* vol. 110, no. 35, pp. 14266-71, Aug 27, 2013.

[12] J. Pascal, C. E. Ashley, Z. Wang *et al.*, "Mechanistic modeling identifies drug-uptake history as predictor of tumor drug resistance and nano-carrier-mediated response," *ACS Nano,* vol. 7, no. 12, pp. 11174-11182, Dec 23, 2013.

[13] Z. Wang, and P. K. Maini, "Editorial: Special Section on Multiscale Cancer Modeling," *IEEE Trans Biomed Eng,* vol. 64, no. 3, pp. 501-503, Mar, 2017.

[14] J. D. Butner, V. Cristini, and W. Zhihui, "Development of a three dimensional, multiscale agent-based model of ductal carcinoma in situ," *Conf Proc IEEE Eng Med Biol Soc,* vol. 2017, pp. 86-89, Jul, 2017.

[15] J. D. Butner, Y. L. Chuang, E. Simbawa *et al.*, "A hybrid agent-based model of the developing mammary terminal end bud," *J Theor Biol,* vol. 407, pp. 259-70, Oct 21, 2016.

[16] M. E. Edgerton, Y. L. Chuang, P. Macklin *et al.*, "A novel, patient-specific mathematical pathology approach for assessment of surgical volume: application to ductal carcinoma in situ of the breast," *Anal Cell Pathol (Amst),* vol. 34, no. 5, pp. 247-63, 2011.

[17] J. Wang, L. Y. Xie, S. Allan *et al.*, "Myc activates telomerase," *Genes Dev,* vol. 12, no. 12, pp. 1769-74, Jun 15, 1998.

[18] Texas Advanced Computing Center (TACC), The University of Texas at Austin.